Atmos. Meas. Tech., 7, 4251–4265, 2014
www.atmos-meas-tech.net/7/4251/2014/
doi:10.5194/amt-7-4251-2014

Atmospheric Measurement Techniques
Open Access

Deployment of a sequential two-photon laser-induced fluorescence sensor for the detection of gaseous elemental mercury at ambient levels: fast, specific, ultrasensitive detection with parts-per-quadrillion sensitivity

D. Bauer[1], S. Everhart[1], J. Remeika[1], C. Tatum Ernest[1,*], and A. J. Hynes[1]

[1]Division of Marine and Atmospheric Chemistry, Rosenstiel School of Marine and Atmospheric Science, University of Miami, 4600 Rickenbacker Causeway, Miami, Florida 33149, USA
[*]currently at: Atmospheric Chemistry Department, Max Planck Institute for Chemistry, Hahn-Meitner-Weg 1, 55128 Mainz, Germany

Correspondence to: A. J. Hynes (ahynes@rsmas.miami.edu)

Received: 21 May 2014 – Published in Atmos. Meas. Tech. Discuss.: 6 June 2014
Revised: 17 September 2014 – Accepted: 30 September 2014 – Published: 8 December 2014

Abstract. The operation of a laser-based sensor for gas-phase elemental mercury, Hg(0), is described. It utilizes sequential two-photon laser excitation with detection of blue-shifted laser-induced fluorescence (LIF) to provide a highly specific detection scheme that precludes detection of anything other than atomic mercury. It has high sensitivity, fast temporal resolution, and can be deployed for in situ measurements in the open atmosphere with essentially no perturbation of the environment. An ambient sample can also be pulled through a fluorescence cell, allowing for standard addition calibrations of the concentration. No type of preconcentration is required and there appears to be no significant interferences from other atmospheric constituents, including gas-phase oxidized mercury species. As a consequence, it is not necessary to remove oxidized mercury, commonly referred to as reactive gaseous mercury (RGM), from the air sample. The instrument has been deployed as part of an instrument intercomparison and compares well with conventional instrumentation that utilizes preconcentration on gold followed by analysis using cold-vapor atomic fluorescence spectroscopy (CVAFS). Currently, the achievable detection sensitivity is $\sim 15\,\mathrm{pg\,m^{-3}}$ ($\sim 5 \times 10^4\,\mathrm{atoms\,cm^{-3}}$, ~ 2 ppq) at a sampling rate of 0.1 Hz, i.e., averaging 100 shots with a 10 Hz laser system. Preliminary results are described for a 50 Hz instrument that utilizes a modified excitation sequence and has monitored ambient elemental mercury with an effective sampling rate of 10 Hz. Additional work is required to produce the precision necessary to perform eddy correlation measurements. Addition of a pyrolysis channel should allow for the measurement of total gaseous mercury (TGM) and hence RGM (by difference) with good sensitivity and time resolution.

1 Introduction

A detailed understanding of the biogeochemical cycling of mercury and the routes to the production of organomercury compounds in ecosystems is a critical issue from a human health perspective. Direct exposure to mercury is primarily through the ingestion of dimethyl mercury from fish consumption; however an understanding of the overall budget and mechanism of chemical transformation of mercury in both its elemental and combined forms is critically important. (U.S. EPA, 2000; Mergler et al., 2007; UNEP, 2008, Diez, 2009). Wet or dry deposition of oxidized mercury is an important step in a complex process that involves both chemistry and microbiology and eventually produces alkyl mercuric compounds. Regulation of anthropogenic mercury sources in the US has almost eliminated emissions from municipal waste combustors and medical waste incinerators and the new "Mercury and Air Toxics Standards" (MATS) will require reductions in mercury emissions from coal-burning power plants (U.S. EPA, 2011). On an international scale the

United Nations Environment Programme has been focused on developing an increased understanding of the global impact of atmospheric mercury (UNEP, 2013). Reductions in mercury emissions have been the focus of global negotiations that have led to the Minimata Convention on Mercury, a multilateral environmental agreement that has been signed by 97 countries (UNEP, 2014). Nevertheless, these developments take place in a situation in which our overall understanding of the chemistry of atmospheric mercury transformation is limited (Hynes et al., 2008; Subir et al., 2011, 2012; Gustin and Jaffe, 2010) . In the absence of a detailed understanding of the atmospheric cycling of mercury, it is quite possible that the desired environmental results will not be attained. For example, emission controls in the USA are designed to try to reduce the wet and dry deposition that ultimately produces increased mercury concentrations in aquatic environments. If this deposition is controlled by oxidation of the global mercury pool, rather than by US anthropogenic emissions, then emission reductions will not decrease deposition.

The typical background concentrations of Hg(0) in unpolluted environments range from 1.5 to 2 ng m^{-3}, where 1 ng m^{-3} is $\sim 3 \times 10^6$ atoms cm^{-3} or ~ 120 ppq (parts per quadrillion), and reactive gaseous mercury (RGM) is thought to be typically less than 10 % of this value; hence atmospheric measurements represent a significant challenge in ultratrace analytical chemistry (Gustin and Jaffe, 2010). It is also important to note that the chemical speciation of oxidized mercury has not been established. Current approaches to the measurement of both elemental and oxidized mercury at ambient levels rely exclusively on instruments that use preconcentration on gold followed by analysis using cold-vapor atomic fluorescence spectroscopy (CVAFS). The issues and problems associated with this approach are discussed by Gustin and Jaffe (2010) and include the question of the extent to which CVAFS instruments are measuring Hg(0) or total gaseous mercury (TGM) or something intermediate between the two. In addition, the necessity to preconcentrate requires a sampling time of minutes for Hg(0) and precludes fast measurements. The current approach to measurement of RGM relies almost exclusively on sampling on KCl-coated annular denuders followed by pyrolysis and CVAFS analysis of the Hg(0) produced by RGM decomposition (Landis et al., 2002).

The development of a fast in situ sensor capable of measuring Hg(0) at ambient levels is a critical research need. Such a sensor can independently verify the performance of the CVAFS instruments. In addition, this type of sensor would offer the possibility of measuring mercury fluxes using a direct micro-meteorological approach: the eddy correlation technique.

We have developed a laser-based sensor for the detection of gas-phase elemental mercury, Hg(0), using sequential two-photon laser-induced fluorescence (2P-LIF). The instrument is capable of fast in situ measurement of Hg(0) at ambient levels. By incorporating pyrolysis to convert RGM to Hg(0), it is possible to measure TGM, and hence RGM by difference. Under atmospheric conditions, the detection of Hg(0) is unambiguous since the sensor can not detect an oxidized mercuric species, irrespective of its chemical speciation, and there are no known atmospheric interferences, i.e., atoms or molecules, that can produce a false positive or artifact signal.

In a prior study we examined four variants of 2P-LIF detection of Hg(0) and performed a detailed laboratory characterization of the spectroscopic characteristics of the most sensitive variant (Bauer et al., 2002, 2003). In this work we describe the performance of a field instrument that uses this approach and was deployed as part of the RAMIX (Reno Atmospheric Mercury Intercomparison Experiment) intercomparison of mercury detection instruments (Gustin et al., 2013). We also show preliminary results from a "second-generation" 2P-LIF system that utilizes a different excitation scheme.

2 Principles of operation

It is instructive to compare the 2P-LIF approach with CVAFS instruments currently used to monitor Hg(0) as exemplified by the Tekran 2537 mercury vapor analyzers (Tekran, 2001). In CVAFS systems, air is pulled through a gold trap that removes gas-phase mercury, forming an amalgam. After a period of sampling the gold trap is flushed with argon and then heated, releasing Hg(0), which flows into a fluorescence cell. A mercury discharge lamp is used to induce fluorescence using the 6^3P_1–6^1S_0 transition at 253.7 nm with detection of resonance fluorescence using a photomultiplier tube (PMT). The key features of the instrument are (i) the gold amalgamation step that selectively removes and preconcentrates gas-phase mercury and (ii) the detection of Hg(0) via resonance fluorescence in the presence of an inert gas that does not quench the 6^3P_1 excited state. The removal of air and use of an inert gas is critical for establishing high sensitivity because O_2 is an extremely efficient quencher of the 6^3P_1 excited state. The 6^3P_1 state has a radiative lifetime of 119 ns and the quenching rate coefficient with O_2 is 3.6×10^{-10} cm^3 $molecule^{-1}$ s^{-1} (Michael and Suess, 1974; Breckenridge and Umemoto, 2007). The fluorescence efficiency in air at atmospheric pressure can be calculated using the Stern–Volmer relationship and gives a fluorescence efficiency of 4.7×10^{-3} and an effective radiative lifetime of 0.56 ns. It should be noted that the quenching efficiency of N_2 is approximately 2 orders of magnitude lower than that of O_2 and that it contributes little to quenching in spite of its higher partial pressure (Deech et al., 1971). Commercial instruments utilizing gold amalgamation typically have detection sensitivities of 0.1 ng m^{-3} based on sampling times of 2.5–5 min. Based on these considerations, it should be clear that while the CVAFS instrumentation is suitable for ambient

monitoring, it is not capable of fast in situ measurements of Hg(0).

The 2P-LIF instrument utilizes two tunable lasers to sequentially pump two atomic transitions in Hg(0) followed by the detection of blue-shifted LIF. The instrument has been deployed in two excitation configurations and the relevant atomic transitions are shown in Fig. 1. In the "first-generation" system the first tunable laser operates at a fundamental wavelength of 507.3 nm and is frequency doubled to produce 253.7 nm exciting the Hg 6^3P_1–6^1S_0 transition. This is followed by excitation with a second laser at 407.8 nm to the 7^1S_0 level via the 7^1S_0–6^3P_1 transition. Both radiative decay and collisional energy transfer produce population in the 6^1P_1 level. Blue-shifted fluorescence is then observed on the strong 6^1P_1–6^1S_0 transition at 184.9 nm using a solar-blind PMT. The first-generation system was deployed at RAMIX. In an effort to investigate the possibility of increasing sensitivity for high-frequency measurements, we have made preliminary measurements using a second-generation system. The second-generation system uses the same Hg 6^3P_1–6^1S_0 transition for the initial excitation, and this is followed by excitation of the 6^3D_1–6^3P_1 transition at 313.2 nm. This fluoresces at 578.9 nm via the 6^3D_1–6^1P_1 transition and again produces population in the 6^1P_1 level. Blue-shifted fluorescence is again observed on the strong 6^1P_1–6^1S_0 transition at 184.9 nm using a solar-blind PMT. The excitation schemes involving sequential excitation of two atomic transitions, followed by detection of the emission from a third, are extremely specific and preclude detection of anything other than Hg(0). In typical single-photon fluorescence systems, including CVAFS, sensitivity is normally limited by the detection of scattered excitation light that occurs at, or is red-shifted relative to, the excitation wavelength. 2P-LIF is detected at 184.9 nm with a solar-blind PMT that has a negligible quantum efficiency above 240 nm, resulting in no detection of the 407.8 and 313.2 nm excitation scatter and minimal response to the 253.7 nm scatter. This leads to the very high sensitivity. A significant added advantage is that the presence of atmospheric aerosols does not significantly degrade detection sensitivity, so it is not necessary to pass the airflow through filters to remove particulates. In systems that utilize resonance fluorescence, even a small particulate loading can dramatically degrade sensitivity because of the increase in scattering of the excitation beam. Similarly, detection approaches using CRDS (cavity ring-down spectroscopy) require filtering because of the attenuation produced by aerosols. In the sequential two-photon system the increase in scatter of the 253.7 and 407.8 nm beams has little impact because these wavelengths are not detected by the PMT. In prior work we examined the linearity, saturation and spectroscopic characteristics of the 2P-LIF system using a high-power "laboratory" laser system consisting of a Nd:YAG laser, dye laser and optical parametric oscillator (Bauer et al., 2002, 2003). Comparison with a Tekran 2537 demonstrated that 2P-LIF is linear over a wide range of Hg(0) concentrations and that the line widths of the excitation transitions were relatively broad. We also examined the saturation characteristics that show the relationship between the power of the excitation beams and the fluorescence signal. The challenge for the ambient environmental monitoring was to produce a relatively compact laser system that would operate reliably for extended periods of time in a mobile trailer.

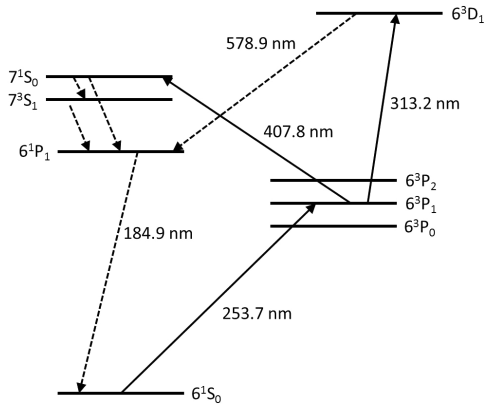

Figure 1. Atomic transitions for Hg(0) that were used in the first- and second-generation detection systems.

3 Description of the mobile instrument

The complete 2P-LIF instrument package deployed for the RAMIX intercomparison was housed in a 20 ft × 8 ft mobile laboratory. Figure 2 shows a block diagram of the experimental setup. A 4 ft × 10 ft optic bench supported the laser systems, optics, and sample cells. The system configuration consisted of two dye lasers (Quanta Ray PDL-2) pumped by a single 10 Hz Nd:YAG laser (Quanta Ray GCR-16). The initial excitation and detection scheme, as discussed above, employed one photon each of 253.7 and 407.8 nm light for the sequential excitation of Hg(0) with the detection of fluorescence at 184.9 nm. The third harmonic of the Nd:YAG laser was split and used to simultaneously pump the two dye lasers. The first laser, using Coumarin 500 dye, operated at a fundamental wavelength of 507.3 nm and was frequency doubled to produce the 253.7 nm excitation photon. The dye was dissolved in methanol with oscillator and amplifier concentrations of 400 and 95 mg L^{-1}, respectively. The typical doubled dye laser output was 1 mJ $pulse^{-1}$. The second dye laser, using Exalite 411 dye, operated at a fundamental wavelength of 407.8 nm, generating the second excitation photon directly. The dye was dissolved in dioxane with oscillator and amplifier concentrations of 150 and 50 mg L^{-1}, respectively. The typical dye laser output was 5 mJ $pulse^{-1}$. In the second-generation system the second dye laser was pumped with the residual second harmonic of the Nd:YAG laser and used DCM dye. The dye was dissolved in methanol with oscillator

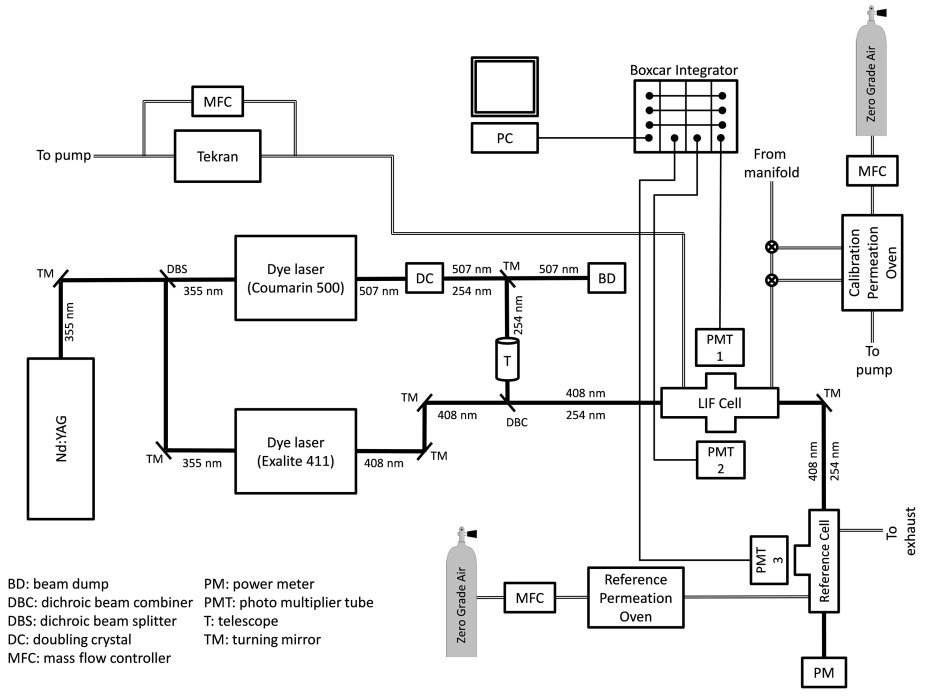

Figure 2. Block diagram of the "first-generation" 2P-LIF system deployed at RAMIX.

and amplifier concentrations of 170 and 24 mg L^{-1}, respectively. The typical doubled dye laser output was 2 mJ $pulse^{-1}$ with 10 Hz pumping and 0.2 mJ $pulse^{-1}$ with 50 Hz pumping. As noted above, the effective radiative lifetime of the 6^3P_1 state is 0.56 ns at atmospheric pressure, which is shorter than the excitation pulse duration of $\sim$6 ns. As a consequence, the population in the 6^3P_1 essentially tracks the temporal profile of the excitation pulse, and accurate synchronization of the excitation pulses is critical. The use of a single pump laser is advantageous because it eliminates the "jitter" associated with the use of two pump lasers. In practice it was found that a slight delay between the two pulses produces optimal sequential excitation. Hence the two beams were spatially overlapped using dichroic optics, and a delay path ensured the 407.8 nm pulse arrived 2–3 ns after the 253.7 nm pulse. In addition, the 253.7 nm beam passed though a 6$\times$ beam expander to reduce the flux and produce better spatial overlap with the 407.8 nm beam. As noted above, typical pulse energies were $\sim$1 mJ at 253.7 nm and 5 mJ at 407.8 nm, and the combined beams, after expansion of the 253.7 nm beam, were $\sim$5 mm in diameter. When sampling was performed in the trailer, the combined beams then passed through a sample cell and a reference cell and then terminated in a beam dump. The sample and reference cells were identical and constructed of 1 in. i.d. Pyrex. They were 12 in. long with two 1 in. side arms attached at the midpoint. O-ring joints (#25) at the ends of both the main cell axis and the side arms allowed for windows to be attached and easily removed for cleaning or exchange. When the sample cell is utilized, air is pulled through a 1/4 in. o.d. Teflon sampling line with an inlet located above the roof of the trailer. No filters are placed on the inlet. If the ambient temperature is significantly above the trailer temperature and the humidity is high, then the sample air is passed through a cold trap, set in an ice bath, to prevent condensation in the sampling lines inside the trailer. For open-air in situ sampling on the trailer roof, the beams pass through the reference cell and are directed by mirrors though a hole in the trailer roof. During RAMIX a single PMT was located on the trailer roof. For sampling with the second-generation system in Miami, two PMTs were located on the trailer roof. After exiting the roof the beam then passed $\sim$1 cm in front of the photocathode of the PMT or PMTs that were located $\sim$3 ft above the trailer roof.

A slow flow ($\sim$100 cc min^{-1}) of zero-grade air passed over a permeation tube located in a temperature-controlled oven, (reference permeation oven in Fig. 2), and provided a stable flow of Hg(0) to the reference cell. The 2P-LIF signal from the sample cell was monitored by two solar-blind PMTs (Hammamatsu) on opposite sides of the sample cell, each aligned perpendicular to the axis of the excitation beams. The use of two PMTs allowed for the dynamic range of the detection system to be increased; increased the number of photons detected; and, as discussed below, allowed for us to distinguish between real fluctuations in Hg(0) concentration and random fluctuations associated with photon statistics. The 2P-LIF signal from the reference cell was monitored by a single PMT aligned perpendicular to the axis of

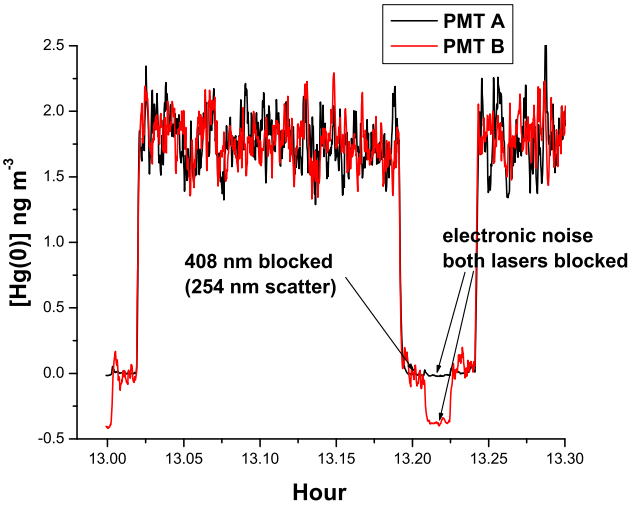

Figure 3. 2P-LIF signal from sample cell collected on 1 September, from the boxcar channels (effective averaging of 70 shots at 10 Hz, i.e., 7 s). Signals from both detection PMTs are shown. The 253.7 nm scattered light and the electronic background noise are labeled.

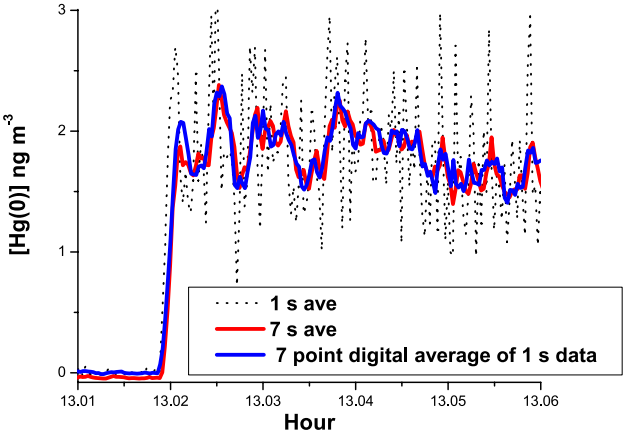

Figure 4. Comparison of 1 s average of 10 Hz data, output of boxcar averaged data, and a 7 s smoothing of the 1 s data.

the excitation beams. The signal from all three PMTs was amplified and processed by boxcar integrators (Stanford Research Systems). Both the single-shot and 100-shot exponential average outputs of the boxcar units were digitized with 13 bit resolution and stored in a computer. The detection efficiency of the solar-blind PMTs drops off significantly for wavelengths longer than 200 nm, so no filters were used to discriminate against background trailer light or laser scatter. Scattered laser light was monitored by taking background measurements in which both the 407.8 and 253.7 nm beams were blocked, giving electronic noise, and then monitoring scatter from both excitation beams separately. Neither PMT saw any scatter from the 407.8 nm excitation beam. A small amount of 253.7 nm scatter was observed, and so only the 253.7 nm scatter was routinely monitored. Figures 3 and 4 display 2P-LIF signals monitoring ambient air, as collected by the computer from the boxcar units; the data are a small section of the 1 and 2 September 2011 data discussed below. Figure 3 shows the boxcar-averaged output for both sample PMTs. The Hg(0) concentration is proportional to the 2P-LIF signal detected when both the 253.7 and 407.8 nm beams are present minus the signal produced by the scattered light from the 253.7 nm laser beam, and the absolute concentration scale has been calibrated as discussed below. The electronic noise and 253.7 nm scatter are labeled in Fig. 3, and it can be seen that the sensitivity of the PMTs to 253.7 nm scatter is different, with tube B seeing significantly more scatter. This is due to the variability in the production of the PMTs. The voltage and hence the gain of the PMTs was adjusted to optimize the sensitivity and dynamic range of the 2P-LIF signal; however, tube B had higher gain and required more frequent adjustment. All data were processed to account for the varying amplification of the PMTs and were then background-subtracted.

In Fig. 4 a 180 s slice of data shows the 1 s average of the 10 Hz single-shot data together with the exponentially averaged output of the boxcar and a 7 s smoothing of the single-shot data. The agreement between the digitally averaged single-shot data and the analogue boxcar average is excellent. It shows that a nominally 100-shot exponential average is essentially equivalent to a 7 s smoothing of the single-shot data.

Either a Tekran 2537A or 2537B mercury analyzer was located downstream from the sample cell and sampled 2 standard liter per minute from the gas flow. The Tekran sampled through a 1μ Teflon particle filter, but no additional filters were used. A mass flow controller (MFC) and diaphragm pump located downstream from the Tekran pulled an additional 8 slpm of air, and so the total flow through the sampling cell was 10 slpm. The sample cell was connected to the RAMIX manifold by 1/4 in. Teflon tubing. The manifold is described in detail by Finley et al. (2013). The sample air could be routed through a second, temperature-controlled, permeation oven ("calibration permeation oven" in Fig. 2) that contained a low-output permeation tube. The temperature was set to produce an addition of typically 5 ng m^{-3} of Hg(0) above ambient, as measured by the Tekran 2537. A constant 10 slpm flow of zero-grade air passed through the calibration permeation oven, except when it was switched into the manifold sampling line for a standard addition to the sample flow. The continuous gas flow ensured oven stability and eliminated the buildup of mercury in the oven. We fabricated both permeation ovens and the permeation tubes. The actual sampling configurations evolved over the course of the campaign and the appropriate specific sampling configurations are described in the Results section.

The instrument has been deployed in Miami, Florida, and Reno, Nevada, and in both places the ambient temperature

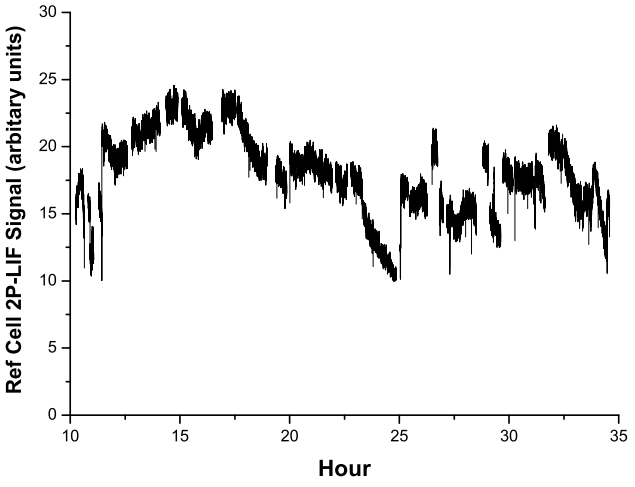

Figure 5. Reference cell signal over a 26 h sampling period on 1 and 2 September.

was well in excess of 30 °C during the day. It was critical to keep the internal trailer temperature at a constant temperature close to 20 °C to ensure stable operation of the laser systems; hence the trailer had three airconditioning units installed.

3.1 Hg concentration units

It has become standard practice in the mercury community to report Hg(0) concentrations in ng m^{-3} referenced to 1 standard atmosphere and 0 °C as these are the concentrations reported by the Tekran 2537 instruments, irrespective of the actual sampling pressure and temperature. As a consequence, these units, rather than being absolute concentrations, effectively report mixing ratios, and a knowledge of the sampling pressure and temperature is required to convert these "mixing ratios" to absolute concentrations. In this paper we will retain this convention using ng m^{-3} referenced to 1 standard atmosphere and 0 °C unless clearly specified otherwise.

3.2 Reference normalization

At the start of a measurement cycle, the excitation dye lasers were optimized to produce the maximum 2P-LIF signal by maximizing output power and then tuning the wavelengths to generate the maximum 2P-LIF signal. At this point the laser wavelengths should be centered on the Hg(0) absorption features, and the 2P-LIF signal will be proportional to the Hg(0) concentration. In practice, both the wavelength and power of the excitation lasers can drift and the sensitivity of the 2P-LIF signal will change. Typically, after an initial startup period, we found the laser systems to be remarkably stable for several hours without requiring adjustment. Nevertheless the power will decrease as the laser dyes degrade and wavelengths can drift as a result of temperature variation and mechanical stability. This is a particular challenge in a mobile laboratory. At the excitation powers used in these experiments, the two atomic transitions are partially saturated and there is no simple relationship between the 2P-LIF signal and the laser powers. Small drifts in wavelength are also difficult to monitor and correct for. To compensate for these drifts, the 2P-LIF signal was monitored in a reference cell that maintained a constant concentration of Hg(0). Any drifts in power or wavelength were then observed as a change in the 2P-LIF signal from the reference cell. The 2P-LIF signal from the sample cell was then normalized to this reference signal. Figure 5 shows the 2P-LIF signal from the reference cell during 26 h of continuous measurement on 1 and 2 September. The reference 2P-LIF signal, which should be constant if the lasers showed no drift, shows fluctuations of 20 % over the first 15 h and then a precipitous drop in power as the dyes degrade. At hour 25, ∼ 01:00 on 2 September, the dyes were changed and the power restored. The reference cell signal also provides a long-term monitor of the performance of the laser and detection systems. In this work, all of the data from ambient samples were background-corrected and then normalized to the reference cell.

We found that changes in crystal alignment and wavelength shifts reducing the 2P-LIF signal by a factor of 5 were corrected by normalizing to the reference cell. However, we have not performed a systematic investigation of the relative responses of the sample and reference systems to changes in power and wavelength drift; we plan to do this as part of any future deployment.

3.3 Calibration

Laser-induced fluorescence is a relative technique since it is not possible to accurately relate the fluorescence signal measured by the PMT to the absolute concentration of the species being monitored. As a consequence, it must be independently calibrated by standard addition of a calibration gas or by comparison with another absolute technique. The 2P-LIF system was calibrated by reference to the Tekran 2537 that was sampling simultaneously from the gas flow. Typically the integrated 2P-LIF signal was referenced to 10 or 15 min of Tekran sampling during each measurement period, and the response of both instruments was compared over the whole measurement period. The Tekran 2537 utilizes a built-in, gravimetrically calibrated Hg(0) permeation tube to calibrate the CVAFS fluorescence signal. Ambient concentrations and spikes were being simultaneously monitored by several Tekran 2537 units; these experiments will be described in detail elsewhere. Furthermore, standard addition of Hg(0) to the sample flow could be introduced by rerouting the sample flow through the calibration permeation oven. We were unable to obtain a gravimetrically calibrated Hg(0) permeation tube prior to RAMIX and, as a result, the standard addition procedure did not offer an independent calibration. However the Tekran and 2P-LIF responses were compared as described below. For future instrument deployments we will utilize a low-output, gravimetrically calibrated

permeation tube to offer an independent absolute calibration of the Hg(0) concentration that will offer an additional check on the Tekran response.

3.4 Instrument response and linearity

The instrument response and linearity of an LIF sensor are dependent on quenching or absorption of the fluorescence signal by atmospheric gases. The Hg 6^3P_1 state that is excited in the first step of the 2P-LIF scheme is quenched very efficiently by O_2, but data are limited on the quenching efficiency of the higher electronic states that are subsequently excited prior to fluorescence. Nevertheless it is reasonable, based on 6^3P_1 quenching rates, to conclude that 2P-LIF fluorescence efficiency is low at atmospheric pressure. In addition, the 184.9 nm fluorescence signal is absorbed by both O_2 and H_2O. The absorption cross sections of O_2 and H_2O are $\sim 1 \times 10^{-20}$ and 7×10^{-20} cm^2 molecule^{-1}, respectively (Creasey et al., 2000). The path length from the 2P-LIF beams to the PMT photocathode is ~ 3 cm, which means that the 184.9 nm bean is attenuated by ~ 15 % by O_2 at atmospheric pressure and by 0.7 % per Torr of H_2O. If both the pressure and gas composition are constant, then both the fluorescence efficiency and the attenuation of the 2P-LIF are constant and the 2P-LIF signal should be proportional to the Hg(0) concentration. If gas composition or pressure are changing significantly, this could produce deviations from linearity. This is a significant issue in the use of 2P-LIF in reactive flows such as combustion or plasma environments, and it could be significant in an aircraft deployment. For ground-based measurements the pressure is constant, and the only potential issue is a change in the H_2O partial pressure. We performed linearity calibrations employing the mobile laser system and using standard addition of Hg(0) to air. We also estimated the effective fluorescence efficiency in our experimental configuration by measuring the relative fluorescence yields in air and He, and we examined the effects of changes in H_2O concentration on the 2P-LIF fluorescence response.

3.4.1 2P-LIF linearity in air

These experiments used an experimental configuration that was identical to that used during the RAMIX intercomparison to compare the 2P-LIF signal with Hg(0) concentrations measured by the Tekran 2537B. A constant flow of zero-grade air passed through a temperature-controlled aluminum oven containing a Teflon mercury permeation tube, supplying a constant amount of Hg(0) into the air stream. The flow was controlled by an MFC. An additional flow of air, controlled by a separate MFC, bypassed the permeation tube and was then added to the permeation oven flow in a mixing line to dilute the Hg(0) concentration and provide variable concentrations for study. Another MFC, backed by a mechanical pump, downstream of the 2P-LIF sample cell, ensured a constant 5.0 slpm flow through the LIF sample cell (including air flow sampled by the Tekran), while a vent line open to ambient atmosphere upstream of the sample cell kept the entire sampling system at atmospheric pressure. The simultaneous detection of Hg(0) using 2P-LIF and Tekran measurements was conducted over a range of 3–18.5 ng m^{-3} by varying the air flow through the dilution line. There is an excellent correlation between the 2P-LIF signal and the Tekran measurements, as shown in Fig. 6 with a least-squares linear regression of the data giving an R^2 of 0.996 and an intercept of 0.06 ± 0.1, i.e., zero within the precision of the measurement. The experiment was then repeated with higher Hg(0) concentrations (12.5–30 ngm^{-3}), and again there was an excellent linear correlation between the 2P-LIF signal and the Tekran measurements: $R^2 = 0.998$ and a zero intercept at a 2σ level of precision. In both cases the variations in concentration were in excellent agreement with those calculated based on the measured dilution. These results verify our prior work in N_2 using the "field instrument" configuration and confirm that, as expected, at constant pressure the 2P-LIF signal varies linearly with Hg(0) concentration in air.

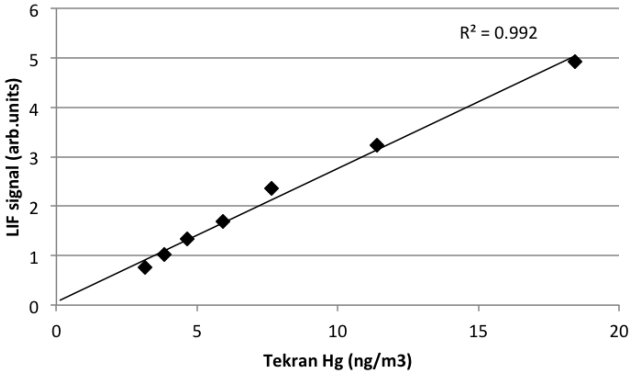

Figure 6. The 2P-LIF signal as a function of Hg(0) concentration measured with the Tekran instrument in zero-grade air together with a calculated regression line.

The relative fluorescence efficiencies in air and He were measured by passing both gases through the permeation oven that was used for standard addition of Hg(0) to sample gases. In this case, zero-grade air or He was used, and the 2P-LIF signal was monitored in each case. The average of these experiments gave a 2P-LIF signal in air that was 3 % of the signal in He. Approximately 15 % of the reduction in signal is due to direct absorption of the 2P-LIF signal by O_2, and the remaining reduction is probably due to enhanced quenching by O_2. Assuming the maximum possible 100 % in He as an example, we would obtain a fluorescence efficiency of approximately 3.5 % in air. As noted above in the low laser power linear fluorescence regime, we would expect a fluorescence efficiency of less than 0.5 % based on quenching of the 6^3P_1 state; additional quenching of the 7^1S_0 and 6^1P_1 states would reduce the fluorescence efficiency even more.

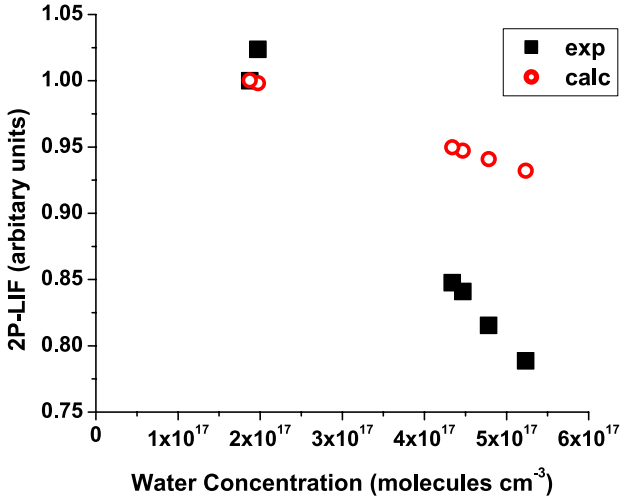

Figure 7. The 2P-LIF signal as a function of H_2O concentration. The calculated points show the expected attenuation based only on absorption of the 2P-LIF signal by H_2O.

While the fluorescence efficiency in He is probably less than 100 %, it is expected to be high. As shown previously, both excitation transitions are partially saturated at the typical powers and laser fluxes used here, and this is likely to explain the higher fluorescence efficiency.

The impact of water vapor was measured by pulling outside air through a water bubbler and measuring the 2P-LIF signal as a function of humidity. Relative humidity was monitored using a humidity sensor and the absolute concentration of water was calculated using the trailer temperature. Figure 7 shows the 2P-LIF signal as a function of water concentration, and it can be seen that the signal drops as the concentration increases. As noted above we expect a decrease in the 2P-LIF signal as a result of absorption by the water vapor, but the observed decrease, shown in Fig. 7 as the "exp" line, is larger than calculated due to absorption alone. There are no literature data on the quenching of excited states of Hg(0) by water, but this result suggests it is also an extremely efficient quencher; this requires further investigation. Typically, the H_2O partial pressure is constant over extended periods of time and the diurnal change in relative humidity is a consequence of temperature change. Nevertheless, we plan to incorporate a humidity measurement downstream of the Tekran and routinely monitor the H_2O partial pressure. We also plan to measure the change in the 2P-LIF signal as a function of the H_2O partial pressure in one atmosphere of air.

4 Interference effects

As we noted above, the 2P-LIF excitation schemes, involving sequential excitation of two atomic transitions followed by detection of the emission from a third, are extremely specific and preclude detection of anything other than atomic mercury. However, it is possible to conceive of interferences, i.e., spurious effects that produce a 2P-LIF Hg(0) signal that does not come from ambient Hg(0). Examples of such interferences include photochemistry coupled with chemistry, the classic example in atmospheric chemistry being the O^1D interference in monitoring ambient OH (Heard and Pilling, 2003). In this case, excitation of OH on the A-X (1-0) band photodissociates O_3, generating O^1D that reacts with water vapor generating OH. Because of the concentration of water vapor in the lower atmosphere and the very fast rate coefficient for this reaction, a single 282 nm laser pulse can generate O^1D and detect the OH product, and this essentially precludes this approach to monitoring tropospheric OH. In the 2P-LIF detection approach the 253.7 nm laser will dissociate ozone, and while most of the O^1D produced will be collisionally relaxed to O^3P followed by recombination to reform O_3, a small fraction will react with water to form OH. The reaction of Hg(0) with OH is very slow, and this will not have any impact on the 2P-LIF measurements (Bauer et al., 2003).

The second type of interference is purely photochemical in which the probe laser photodissociates a parent molecule, producing, as a photofragment, the molecule or atom under study. An example of such an interference appeared in early attempts to monitor H atoms in flames using two-photon excitation at 205 nm (Goldsmith, 1986). It became clear that the two-photon LIF signal did not reflect the nascent H atom concentrations in the flames but was in fact produced by the photodissociation of water vapor. Photolysis of oxidized mercury compounds such as $HgCl_2$ and $HgBr_2$ can produce some Hg(0) photofragments; however the absorption cross section for Hg(0) is approximately 3 orders of magnitude greater than that of HgX_2 compounds at 253.7 nm and under ambient conditions the concentration of HgX_2 is normally much lower than Hg(0) (Templet et al., 1972; Maya, 1977). We will discuss the interference tests conducted during RAMIX campaign elsewhere, but it should be noted that there are no potential effects in monitoring ambient Hg(0). This is not necessarily the case in reacting combustion flows; in an environment in which most of the mercury is present as Hg(II), the photochemical interference could become significant.

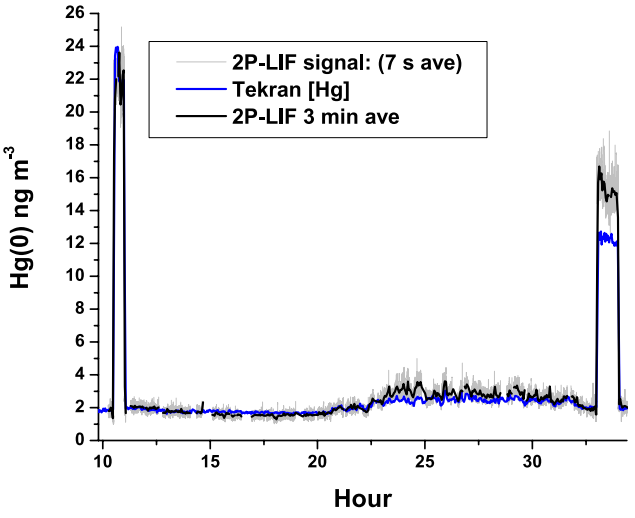

Figure 8. 2P-LIF and Tekran signals over a 26 h sampling period on 1 and 2 September. The Tekran samples every 2.5 min. The 7 s boxcar output is shown together with a 3 min smoothing of the boxcar output.

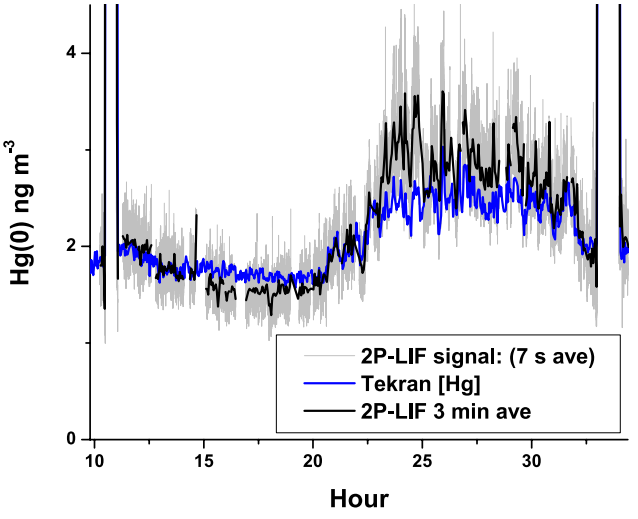

Figure 9. LIF and Tekran signals over a 26 h sampling period on 1 and 2 September. The Tekran samples every 2.5 min. The 7 s boxcar output is shown together with a 3 min smoothing of the boxcar output. The concentration scale is expanded to show the ambient data more clearly.

5 Results

5.1 General overview

For the RAMIX intercomparison the mobile lab was towed from Miami to Reno, a 3000-mile journey, in August 2011. After arrival in Reno it took approximately 3 days to hook up utilities, set up the lab and begin taking data. For most of the intercomparison we sampled from the RAMIX manifold, which was designed to allow for simultaneous sampling by the four RAMIX participants and also by the University of Nevada, Reno (UNR), host group. The manifold is described in detail by Finley et al. (2013). During the RAMIX campaign we sampled on 18 days, typically sampling for between 4 and 6 h. The longest period of continuous sampling lasted for 26 h and occurred on 1 and 2 September. Over this 18-day period we sampled from the RAMIX manifold, and, in addition, at the end of the campaign we sampled ambient air independently and also attempted to measure RGM by pyrolyzing the sample air and measuring the difference between Hg(0) and TGM. During this period the ambient air sampled by the RAMIX manifold was spiked with additional known concentrations of Hg(0), RGM(HgBr2), H_2O, and O_3 both separately and concurrently. The RAMIX results, including a detailed comparison with multiple Tekran instruments, the interference tests and the preliminary attempts to measure RGM, will be described elsewhere. Here we focus on the overall instrument performance, derived limits of detection and, in addition, the preliminary results from 10 Hz and 50 Hz systems utilizing the 313.2 nm, 6^3D_1–6^3P_1 transition for the second excitation photon.

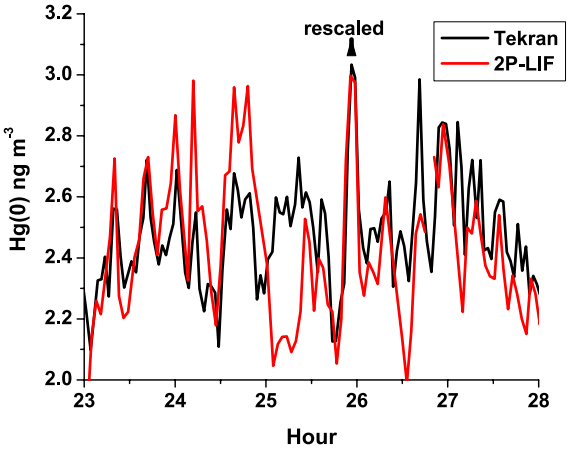

Figure 10. An expanded section of the 1–2 September sampling period showing the nighttime variation in Hg(0) concentration detected by the Tekran and 2P-LIF instruments. The 2P-LIF data are rescaled to the labeled peak.

5.2 Extended sampling

The quality of the data during an extended operation can be gauged from data obtained on 1 and 2 September, when we were able to perform 26 h of continuous sampling. Figures 8 and 9 show the full sampling period, which began shortly before 10:00 on 1 September. The x axis shows the hour after midnight on 31 August in local time in Reno, and the y axis shows the measured concentrations in ng m^{-3} as measured by the Tekran 2537B. Since the 2P-LIF measurement gives a relative response, it is necessary to calibrate the 2P-LIF signal using the Tekran. The data prior to hour 11, including the

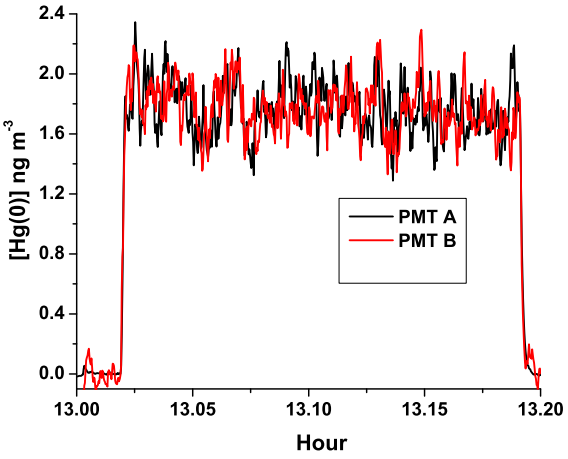

Figure 11. 2P-LIF signals from the two individual boxcar channels over a 10 min sampling period at ∼ 13:00 local time on 1 September.

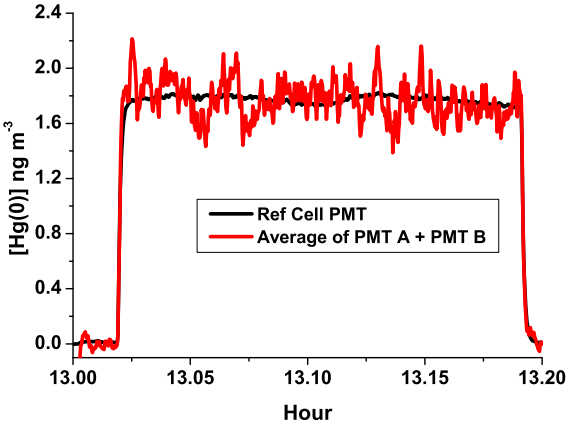

Figure 12. Average of the 2P-LIF shown in Fig. 11 together with the reference cell signal normalized to the same amplitude.

initial large manifold spike of Hg(0) at ∼hour 10.5, were calibrated relative to 10 min of ambient Tekran sampling at hour 10.2. At hour 11 the 253.7 nm turning mirror was bumped; therefore a realignment of the beams was required. Hence, for the remaining 25 h of sampling, the 2P-LIF signal was calibrated relative to 10 min of ambient Tekran measurements at hour 13.1, shortly after 13:00 on 1 September. The Tekran signal is a 2.5 min average; the 2P-LIF signals are the average of the boxcar outputs, effectively a 7 s average of 10 Hz data and a 3 min smoothing of that data, which makes it easier to track the differences between the Tekran and 2P-LIF signals. The 2P-LIF signals from each PMT have been corrected for laser background as well as changes in gain when PMT voltages were adjusted and then normalized to changes in the reference cell signal. The average of these two background-corrected signals was then taken. Figure 9 shows the full sampling record for the 26 h sampling period but with an expanded concentration scale. We began taking data shortly before 10:00 and saw the 10:00 elemental mercury spike that was added to the RAMIX manifold. At hour 33, corresponding to 09:00 on 2 September, we also saw the manifold spike, and shortly after that we stopped sampling from the manifold. The expanded concentration scale in Fig. 9 shows the ambient air signal more clearly, and we see a diurnal variation in the Hg(0) concentration that is captured in both the 2P-LIF and Tekran data. Figures 8 and 9 show that there are issues in the scaling of the signals and that the 2P-LIF and Tekran signals are not responding in an absolutely linear fashion with respect to each other. We had significant problems with the response and calibration of the Tekran 2537B, which we suspect are due to the large drop in pressure between the manifold and sampling cell. For this data set we find that calibrating the 2P-LIF signal using the UNR Tekran data at the second spike produces better agreement over the 26 h sampling period. In the figures the gaps in the 2P-LIF signal typically correspond to 3 min gaps when laser background signals were recorded. In these plots, these periods were set equal to zero. If we examine a 5 h period during the night, we see significant fluctuations that are captured by both the 2P-LIF and Tekran instruments; however the concentration scaling is an issue. Figure 10 shows the 2P-LIF data rescaled to the Tekran concentration at a concentration peak that occurs shortly before hour 26.2 on 2 September; we see reasonable but certainly not perfect agreement in the fluctuations in Hg(0) concentration. As noted above, we see better agreement over the 26 h sampling period if we normalize to the UNR Tekran. On 5 September the 2P-LIF instrument sampled for 7 h, and on this day there was excellent agreement between three independently operated Tekran instruments and the normalized 2P-LIF signal, including two large manifold Hg(0) spikes. We will address the issues of variability between the Tekran and 2P-LIF instruments elsewhere. Nevertheless, we conclude that both instruments are clearly measuring Hg(0).

The 2P-LIF instrument shows short-term temporal variations in Hg(0) concentration and it is important to determine how much of the variation reflects actual changes in the Hg(0) concentration in the atmosphere as opposed to statistical noise in the 2P-LIF signal. This is important in evaluating the RAMIX data set and critical in evaluating the feasibility of eddy correlation measurements with this system. Ideally we could assume that, after laser-related fluctuations are corrected with the reference signal, features that are correlated between the two PMTs reflect a real variation in the Hg(0) concentration. However the difference in the susceptibility of the two PMTs to the 253.7 nm scatter makes this somewhat problematic. Figure 11 shows a greatly expanded timescale capturing 10 min of continuous sampling at hour 13. This is the section of the data set that was used to calibrate the 2P-LIF signals for the period from hour 11 to 36 by normalizing the integral of the 10 min 2P-LIF signals to the Tekran concentration. The figure shows the two individual boxcar outputs, i.e., 7 s averages of the 10 Hz sig-

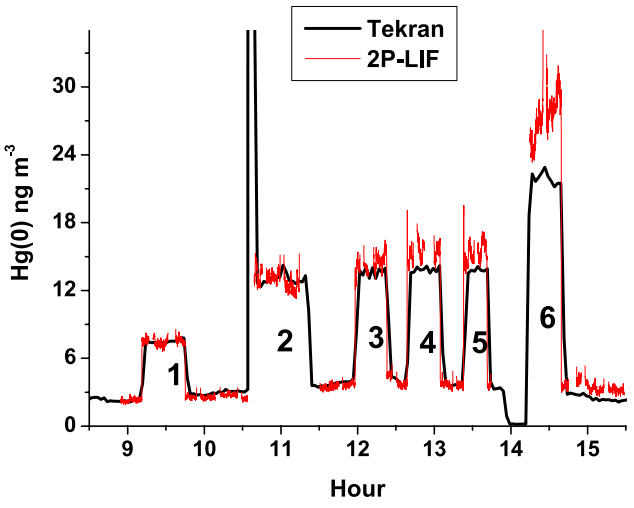

Figure 13. Data from 8 September showing ambient concentration, manifold spikes (1,6) , and in situ 2P-LIF calibration using permeation oven additions (2, 3, 4, 5).

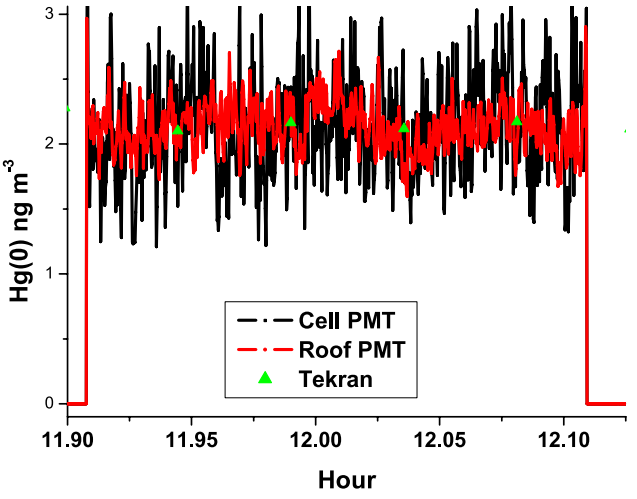

Figure 14. Comparison of 2P-LIF signals from PMTs located on the trailer roof and the sample cell. The signals are normalized to the concentrations measured by the Tekran. Data from 16 September at approximately noon.

nals. Figure 12 shows the average of the two signals and the reference cell output normalized to the same amplitude as PMTs A and B. It is apparent that there are fluctuations on a 7 s timescale that are captured by both 2P-LIF PMTs, but some of the fluctuations are not correlated. The comparison with the reference cell output shown in Fig. 12 demonstrates that the variation in the ambient 2P-LIF signal is not due to pulse-to-pulse or short-term wavelength variations in the probe lasers. There is almost no variation in the reference cell 2P-LIF signal during this period. In fact, the mean of the normalized signals is 1.7 ng m^{-3} and the 1σ variation in the signals is 0.18, 0.17 and 0.03 ng m^{-3} for PMT A, PMT B and the reference PMT, respectively. In contrast, the 1σ variation in the 253.7 nm scatter is 0.012 ng m^{-3} for PMT A and 0.071 ng m^{-3} for PMT B. Based on this we might conclude that the fluctuations we see in the PMT A signal are real; however we know that the quantum efficiencies of the solar-blind PMTs are very low, $\sim$ 0.1 %, and so we do not detect many photons per shot. The shot noise associated with sampling 70 laser pulses would be $\sim$ 12 % detecting 1 photon per pulse and $\sim$ 2 % detecting 25 photons per pulse. This is the 1σ deviation in the magnitude of the signal that is assumed to be proportional to the number of photons detected. Hence it seems reasonable that at least some of the uncorrelated variations in the ambient Hg(0) signals from PMTs A and B are likely to be a result of photon statistics.

5.3 Permeation oven calibrations

Figure 13 shows data from 8 September, when we attempted an in situ calibration using permeation oven additions. On this day there were additional manifold spikes of Hg(0) at $\sim$ 9 and 14 h and also ongoing manifold spikes of water and $HgBr_2$. In Fig. 13 the manifold spikes are labeled as 1 and 6, and the agreement between the values reported by the UM, UW and UNR Tekrans was good. The inline Hg(0) additions are labeled as 2, 3, 4 and 5. The figure shows a comparison of the 2P-LIF and Tekran data with the 2P-LIF signal calibrated to manifold addition 1 at $\sim$ 09:00 It can be seen that, over the course of the 6 h of sampling, the 2P-LIF signal is drifting upward relative to the Tekran output. The integrated additions from the Tekran give an average addition of 9.7 ng m^{-3} for peak 2, rising to 10.3 ng m^{-3} for peak 5, and the concentrations for peaks 1 and 6 agree well with the other independent Tekran measurements. This suggests that the oven is not completely stable, with an output that rises by $\sim$ 6 % over 3,h. It also implies that the discrepancy between the measurements is a result of problems with the 2P-LIF response. A closer examination of the 2P-LIF signal shows that the upward divergence is a result of the normalization procedure, i.e., a significant drop in the reference cell signal. We also found that there is some drift in the individual channels, i.e., the individual PMT outputs. This could be a result of problems with one or both of the PMTs or the cell windows but is more likely due to drifts in the signal processing electronics; this needs to be examined in more detail.

5.4 Trailer rooftop sampling at RAMIX

On the final day of the RAMIX experiment we sampled directly on the trailer roof, placing a PMT approximately 3 ft above the trailer roof. The laser beams were directed through the sampling and reference cells within the trailer and were reflected vertically, passing through a hole in the trailer roof. The sample cell in the trailer was switched between a sample line located on the roof next to the roof PMT and the RAMIX manifold. This enabled us to perform direct, in situ 2P-LIF

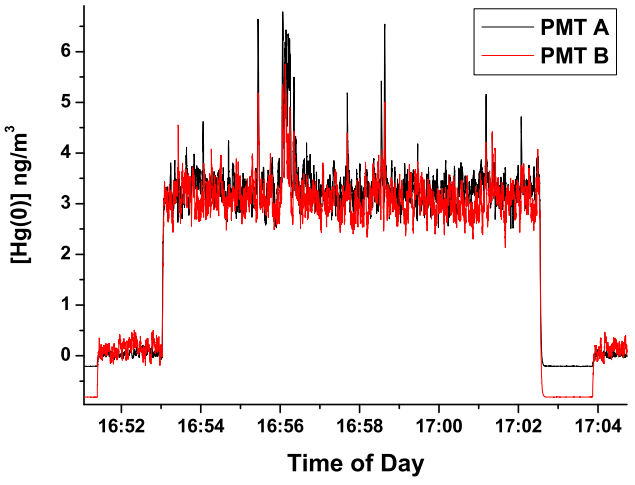

Figure 15. 2P-LIF signal from two individual boxcar channels with 253.7 nm/313.2 nm excitation scheme using a 10 Hz laser system. The figure shows a 10 min slice of a 1 h sample.

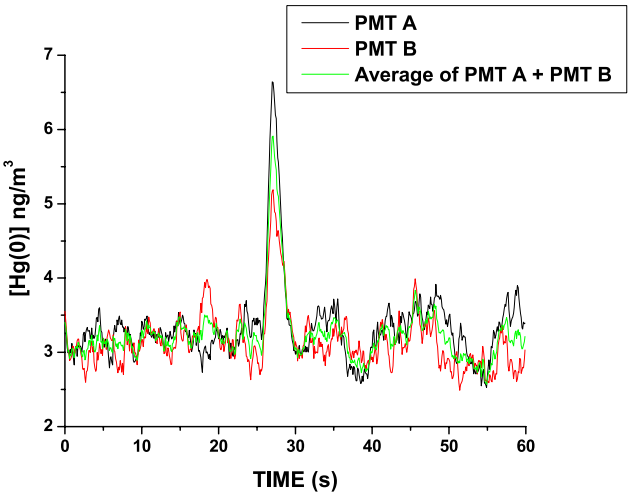

Figure 16. 2P-LIF signal with 253.7 nm/313.2 nm excitation scheme showing data from Fig. 15 on an expanded scale, specifically the feature at hour 16.55. A 1 min section of data is shown; the scale is in seconds. The individual boxcar channels and their average are shown.

measurements of the air above the trailer while simultaneously using a sampling line to pull air into the sample cell for 2P-LIF measurements inside the trailer. It is worth noting that the PMTs require no type of optical filter; hence the roof PMT had the excitation laser beams passing directly in front of the bare photocathode that was directly exposed to both laser scatter and sunlight.

The PMT on the sample cell was approximately 5 cm from the excitation lasers, constrained by the length of the sample cell side arms. Since the number of photons collected varies inversely as the square of the distance of the photocathode from the excitation beams, there is a significant advantage in working in ambient air with no sample cell. Firstly, there is an increase in signal because the PMT is closer to the excitation beam. Secondly, there is no 253.7 nm scatter from the cell windows. Figure 14 shows a comparison of the 2P-LIF signals from the PMTs on the roof and in the sample cell. The signals are calibrated by the Hg(0) concentration measured by the Tekran after the sample cell. The fluctuations in the 2P-LIF signal from roof PMT are significantly smaller than the fluctuations in the cell PMT. This is consistent with the conclusion that these fluctuations are related to the limited number of photons collected.

5.5 2P-LIF using excitation of the 6^3D_1–6^3P_1 transition

In an effort to increase the fluorescence photon flux, we have investigated an alternate excitation scheme in which we pump the 6^3D_1–6^3P_1 transition at 313.2 nm as the second step in sequential excitation. The 6^3D_1 level then fluoresces via the 6^3D_1–6_1P_1 transition at 578.9 nm, populating the 6^1P_1 level. As before, we monitor fluorescence from the 6^1P_1–6^1S_0 transition at 184.9 nm. The experiment is similar to that described previously; however we now use the residual second harmonic of the Nd:YAG laser to pump a dye laser operating with DCM dye $\sim$ 626.4 nm. The 626.4 nm is then frequency-doubled in a KPD crystal, producing the 313.2 nm excitation photon. This scheme allows us for to use the additional residual power at 532 nm that is not utilized in the first excitation configuration, but it requires the second dye laser to be frequency-doubled. Fig. 15 shows an example of data collected on the Rosenstiel School (RSMAS) campus with the trailer located next to the campus dock. The PMTs are located on the trailer roof, so no sampling cell is used. The air close to the PMTs was sampled using the Tekran to put the 2P-LIF signals on an absolute concentration scale. The data were obtained using the 10 Hz Nd:YAG laser to pump the dye lasers. Figure 16 has an expanded x axis showing a 1 min segment of the data and includes the individual PMT outputs and their average with the time axis in seconds. It can again be seen that an examination of the correlation between the 2P-LIF signals from two PMTs is useful for seeing the difference between real fluctuations in the Hg(0) concentration and noise from photon statistics. For example, it is clear that the feature at 16:55:26 showing an $\sim 3\,\mathrm{ng\,m^{-3}}$ spike in the Hg(0) concentration is real. This feature has a width at half maximum of $\sim$ 3 s and again demonstrates the ability of the instrument to capture a very rapid fluctuations in Hg(0) concentration at ambient levels. We never saw this type of fluctuation during RAMIX, and these observations, with a location close to the RSMAS dock overlooking Biscayne Bay, are interesting.

Figure 17 gives an example of the current performance of the 50 Hz system, taking 5-shot averages to give an effective sampling rate of 10 Hz.

Table 1. Typical detection sensitivities.

λ_2 nm	λ_{254} power mJ	λ_2 power mJ	Rep. rate	[Hg] ng m^{-3}	Detection sensitivity (10 s) pg m^{-3}
407.8	0.6	4	10	2.5	30
313.2	1	2	10	2.5	15
313.2	0.7	0.2	50	2.5	35

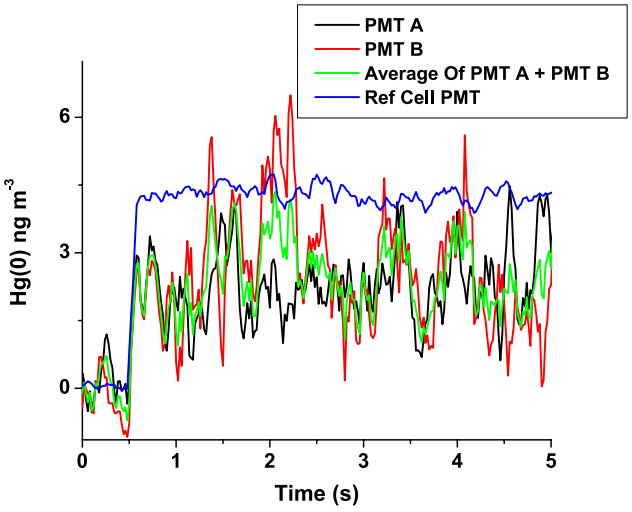

Figure 17. 2P-LIF ambient sample using 50 Hz laser system, taking 5-shot averages to give an effective sampling time of 10 Hz. The figure shows a 5 s slice of data giving the outputs of PMT A, PMT B, their average and the reference cell.

The figure shows a 5 s slice of data giving the outputs of PMT A, PMT B, their average and the reference cell. We see rapid variation in the ambient signal that is not present in the reference cell signal, indicating that these fluctuations are not due to instrumental artifacts. However, we again see that some of the fluctuations are not correlated between the two PMTs, suggesting that the fluctuations are, at least in part, a reflection of the photon statistics. We believe that a significant increase in the power of the 313.2 nm excitation beam is possible and that we can also increase the number of detection PMTs to increase the number of photons collected and improve the photon statistics.

5.6 Detection sensitivity

We have used the 253.7 nm/407.8 nm detection at 10 Hz and the 253.7 nm/313.2 nm excitation scheme with both the 10 and 50 Hz laser systems. The use of the 50 Hz system in the mobile laboratory is somewhat more challenging because of the sensitivity of the Nd:YAG pump laser to temperature fluctuations. In addition, we have relatively limited experience in the use of the PDL dye lasers with 50 Hz pumping and we saw a very large decrease in the output power at 313.2 nm as compared to the decrease at 253.7 nm. Table 1 shows an example of the limits of detection (LODs) that we have achieved through examination of the 10 Hz data from RAMIX with 253.7 nm/407.8 nm excitation and using both 10 and 50 Hz pump lasers with the 253.7 nm/313.2 nm excitation scheme with the mobile laboratory located at RSMAS close to Biscayne Bay. The analysis examined blocks of data that were taken contiguously with typically 5–10 min of signal with 1 min of background sampling before and after. The LOD is a 2σ measure of the standard deviation in the background scatter. The limits of detection we have achieved with the 313.2 nm scheme are comparable to those achieved using 407.8 nm. As a practical matter, the advantages associated with the use of a red dye in methanol solution with a long lifetime compared with the use of an Exalite dye in dioxane solution are significant and outweigh the disadvantage of having to frequency-double. The detection limits we have achieved after a relatively short period of time are comparable to those achieved with the 407.8 nm system after several years of development. At the moment, the large drop in 313.2 nm power associated with the switch to 50 Hz pumping is significantly limiting our detection sensitivity, and we expect to achieve a considerable gain in sensitivity if we can improve the 313.2 nm output.

6 Measurement of total gaseous and reactive gaseous mercury

It is worth noting that the detection sensitivities achieved here suggest that adding a second analysis cell and using pyrolysis to measure TGM could allow us to measure RGM by difference with sufficiently high sensitivity to make ambient measurements if we average for 30 s. We made preliminary measurements of TGM using pyrolysis during RAMIX, and these measurements will be described elsewhere.

7 Comparison with other techniques

As noted above, CVAFS techniques are currently the standard approach to the measurement of Hg(0) and TGM. As has been discussed by Gustin and Jaffe (2010), the extent to which CVAFS systems measure some fraction of RGM is an issue that requires resolution. However, it is clear that these systems require preconcentration and are not capable of fast

in situ determination of Hg(0). Pierce et al. (2013) provide a review of CRDS and other mercury sensors that might offer an alternative to CVAFS. Faïn et al. (2010) proposed that CRDS is capable of fast in situ measurements and reported a detection sensitivity of 0.1 ng m^{-3} with a 10 s time resolution. In more recent work, the same group appears to have acknowledged that, because of O_3 interference, in situ measurements of Hg(0) are not feasible using CRDS and that the sample needs to be stripped of ozone before introduction into the CRDS cavity (Pierce et al., 2013). Under these conditions they report a detection sensitivity of 0.35 ng m^{-3} with an integration time of 5 min. The ozone is stripped from the ambient sample by pyrolysis, which may convert RGM to Hg(0); therefore any RGM must be removed before pyrolysis. It appears that the CRDS technique is not capable of the sensitivity and time resolution currently achievable with CVAFS instruments, and it is unlikely to be useful for fast in situ measurements of Hg(0) at typical ambient levels.

8 Conclusions

We have described the deployment of a laser-based sensor for gas-phase elemental mercury that has high sensitivity and fast temporal resolution. The sensor can be deployed for in situ measurements in the open atmosphere with essentially no perturbation of the environment. An ambient sample can also be pulled through a fluorescence cell, allowing for standard addition calibrations of the concentration. No type of preconcentration is required, and there appear to be no significant interferences from other atmospheric constituents, including gas-phase oxidized mercury species. As a consequence, it is not necessary to remove RGM from the sample. Currently achievable detection sensitivity is ~ 15 pg m^{-3} ($\sim 5 \times 10^4$ atoms cm^{-3}, ~ 2 ppq) with a 10 s detection time. The instrument has operated with an effective time resolution of 10 Hz, but additional work is required to produce the precision necessary to perform eddy correlation measurements. Addition of a pyrolysis channel should allow for the measurement of TGM and hence RGM (by difference) with good sensitivity and time resolution.

Acknowledgements. This work was supported through a National Science Foundation Major Instrumental Grant (#MRI-0821174), through NSF grant # AGS-1101965 and by the Electric Power Research Institute. We thank Mae Gustin and her research group for their hospitality and assistance during the RAMIX intercomparison.

Edited by: D. Heard

References

Bauer, D., Campuzano-Jost, P., and Hynes, A. J.: Rapid, ultrasensitive detection of gas phase elemental mercury under atmospheric conditions using sequential two-photon laser induced fluorescence, J. Environ. Monitor., 4, 339–343, 2002.

Bauer, D., D'Ottone, L., Campuzano-Jost, P., and Hynes, A. J.: Gas Phase Elemental Mercury: A Comparison of LIF Detection Techniques and Study of the Kinetics of Reaction with the Hydroxyl Radical, J. Photochem. Photobiol. A, 157, 247–256, doi:10.1016/S1010-6030(03)00065-0, 2003.

Breckenridge, W. H. and Umemoto, H.: Collisional Quenching of Electronically Excited Metal Atoms, in Advances in Chemical Physics: Dynamics of the Excited State, Volume 50, edited by: Lawley, K. P., John Wiley & Sons, Inc., Hoboken, NJ, USA, doi:10.1002/9780470142745.ch5, 2007.

Creasey, D. J., Heard, D. E., and Lee, J. D.: Absorption cross-section measurements of water vapour and oxygen at 185 nm. Implications for the calibration of field instruments to measure OH, HO_2 and RO_2 radicals, Geophys. Res. Lett., 27, 1651, doi:10.1029/1999GL011014, 2000.

Deech, J. S., Pitre, J., and Krause, L.: Quenching and Depolarization of Mercury Resonance, Can. J. Phys., 49, 1976–1981, 1971.

Diez, S.: Human health effects of methylmercury exposure, Rev. Environ. Contam. T., 198, 111–132, doi:10.1007/978-0-387-09647-6_3, 2009.

Faïn, X., Moosmüller, H., and Obrist, D.: Toward real-time measurement of atmospheric mercury concentrations using cavity ring-down spectroscopy, Atmos. Chem. Phys., 10, 2879–2892, doi:10.5194/acp-10-2879-2010, 2010.

Finley, B. D., Jaffe, D. A., Call, K., Lyman, S. N., and Gustin, M.: Development, testing, and deployment of an air sampling manifold for spiking elemental and oxidized mercury during RAMIX, Environ. Sci. Technol., 47, 7277–7284, doi:10.1021/es304185a, 2013.

Goldsmith, J. E. M.: Photochemical Effects in 205 nm, Two. Photon-Excited Fluorescence Detection of Atomic Hydrogen. Flames, Opt. Lett., 11, 416–418, 1986.

Gustin, M. and Jaffe, D.: Reducing the Uncertainty in Measurement and Understanding of Mercury in the Atmosphere, Environ. Sci. Technol., 44, 2222–2227, 2010.

Gustin, M. S., Huang, J., Miller, M., Peterson, C., Jaffe, D., Ambrose, J., Finley, B., Lyman, S., Call, K., Talbot, R., Feddersen, D., Mao, H., and Lindberg, S.: Do We Understand What the Mercury Speciation Instruments Are Actually Measuring? Results of RAMIX, Environ. Sci. Technol., 47, 7295–7306, doi:10.1021/es3039104, 2013.

Heard, D. E. and Pilling, M. J.: Measurement of OH and HO_2 in the troposphere, Chem. Rev., 103, 5163–5198, 2003.

Hynes, A. J., Donohoue, D. L., Goodsite, M. E., and Hedgecock, I. M.: Our current understanding of major chemical and physical processes affecting mercury dynamics in the atmosphere and at the air-water/terrestrial interfaces, in: Mercury Fate and Transport in the Global Atmosphere, edited by: Mason, R. and Pirrone, N., Springer Science, 427–457, doi:10.1007/978-0-387-93958-2_14, New York, NY, 2009.

Landis, M. S., Stevens, R. K., Schaedlich, F., and Prestbo, E. M.: Development and Characterization of an Annular Denuder Methodology for the Measurement of Divalent Inorganic Reac-

tive Gaseous Mercury in Ambient Air, Environ. Sci. Technol., 36, 3000–3009, 2002.

Maya, J.: Ultraviolet absorption cross sections of HgI_2, $HgBr_2$, and tin (II) halide vapors, J. Chem. Phys., 67, 4976, doi:10.1063/1.434681, 1977.

Mergler, D., Anderson, H. A., Chan, L. H. M., Mahaffey, K. R., Murray, M., Sakamoto, M., and Stern, A. H.: Methylmercury exposure and health effects in humans: A worldwide concern, Ambio., 36, 3–11, 2007.

Michael, J. V. and Suess, G. N.: Absolute Quenching Cross-Sections of Hg (^{3}P) with various molecules, J. Phys. Chem., 78, 482–487, 1974.

Pierce, A., Obrist, D., Moosmüller, H., Faïn, X., and Moore, C.: Cavity ring-down spectroscopy sensor development for high-time-resolution measurements of gaseous elemental mercury in ambient air, Atmos. Meas. Tech., 6, 1477–1489, doi:10.5194/amt-6-1477-2013, 2013.

Subir, M., Ariya, P. A., and Dastoor, A. P.: A review of uncertainties in atmospheric modeling of mercury chemistry I. Uncertainties in existing kinetic parameters : Fundamental limitations and the importance of heterogeneous chemistry, Atmos. Environ., 45, 5664–5676, 2011.

Subir, M., Ariya, P. A., and Dastoor, A. P.: A review of the sources of uncertainties in atmospheric mercury modeling II. Mercury surface and heterogeneous chemistry – A missing link, Atmos. Environ., 46, 1–10, 2012.

UNEP Chemicals Branch: The Global Atmospheric Mercury Assessment: Sources, Emissions and Transport, UNEP-Chemicals, Geneva, Switzerland, 2008.

Templet, P., McDonald, J. R., McGlynn, S. P., Kendrow, C. H., Roebber, J. L., and Weiss, K.: Ultraviolet Absorption Spectra of Mercuric Halides, J. Chem. Phys., 56, 5746, doi:10.1063/1.1677111, 1972.

UNEP: United Nations Environment Program, Chemicals Branch, The Global Atmospheric Mercury Assessment: Sources, Emissions and Transport, ISBN: 978-92-807-3310-5, UNEP Chemicals Branch, Geneva, Switzerland, 2008.

UNEP: Global Mercury Assessment 2013: Sources, Emissions, Releases and Environmental Transport, UNEP Chemicals Branch, Geneva, Switzerland 2013.

UNEP: United Nations Environment Program, available at: http://www.mercuryconvention.org (last access: 5 November 2014), 2014.

U.S. EPA: United States Environmental Protection Agency "Mercury Research Strategy", EPA/600/R-00/073, September 2000.

U.S. EPA: Memorandum: Emissions Overview: Hazardous Air Pollutants in Support of the Final Mercury and Air Toxics Standard, U.S. EPA, EPA-454/R-11-014, available at: http://www.epa.gov/mats/pdfs/20111216EmissionsOverviewMemo.pdf (last access: 5 November 2014), 2011.